Phys Chem Minerals (2011) 38:311–319
DOI 10.1007/s00269-010-0405-0

ORIGINAL PAPER

Solid solution behaviour of $CaSiO_3$ and $MgSiO_3$ perovskites

Daniel Y. Jung · Max W. Schmidt

Received: 19 February 2010 / Accepted: 8 October 2010 / Published online: 26 October 2010

Abstract Using density functional simulations within the generalized gradient approximation and projector-augmented wave method together with thermodynamic modelling, the reciprocal solubilities of $MgSiO_3$ and $CaSiO_3$ perovskites were calculated for pressures and temperatures of the Earth's lower mantle from 25 to 100 GPa and 0 to 6,000 K, respectively. The solubility of Ca in $MgSiO_3$ at conditions along a mantle adiabat is found to be less than 0.02 atoms per formula unit. The solubility of Mg in $CaSiO_3$ is even lower, and most important, the extent of solid solution decreases with pressure. To dissolve $CaSiO_3$ perovskite completely in $MgSiO_3$ perovskite, a solubility of 7.8 or 2.3 mol% would be necessary for a fertile pyrolytic or depleted harzburgitic mantle, respectively. Thus, for any reasonable geotherm, two separate perovskites will be present in fertile mantle, suggesting that Ca-perovskite will be residual to low degree melting throughout the entire mantle. At the solidus, $CaSiO_3$ perovskite might completely dissolve in $MgSiO_3$ perovskite only in a depleted mantle with <1.25 wt% CaO. These implications may be modified if Ca solubility in $MgSiO_3$ is increased by other major mantle constituents such as Fe and Al.

Keywords Ab initio calculations · Solid solutions · Earth's mantle · Earth interior structure and properties

D. Y. Jung (✉)
Laboratory of Crystallography, ETH Zurich,
Wolfgang-Pauli-Str. 10, 8093 Zurich, Switzerland
e-mail: daniel.jung@mat.ethz.ch

M. W. Schmidt
Institute of Geochemistry and Petrology, ETH Zurich,
Clausiusstrasse 25, 8092 Zurich, Switzerland

Introduction

Under the assumption that the Earth's lower mantle is pyrolytic and isochemical to the upper mantle, (Mg,Fe)SiO_3 perovskite (~70%) is thought to be the most abundant phase in the lower mantle, followed by magnesiowüstite (Mg,Fe)O with ~20% and $CaSiO_3$ with between 6 and 12 vol% (Anderson 1989; O'Neill and Jeanloz 1990). One of the open questions concerning Ca in the lower mantle is whether with increasing temperature and depth, the entire amount of Ca could be incorporated into $MgSiO_3$ perovskite such that the $CaSiO_3$ perovskite phase would vanish. This would happen if $MgSiO_3$ perovskite would incorporate 7.8 mol% Ca for a fertile pyrolytic mantle or 2.3 mol% for a depleted harzburgitic mantle (Anderson 1989; Green et al. 1979), the former being considerably more than the 2.0–3.2 mol% Ca reported from experiments on the uppermost portions of the lower mantle (Taura et al. 2001; Hirose et al. 2004; Ono et al. 2001).

$CaSiO_3$ perovskite itself has been of interest in a wide range of studies. Experimental investigations show that various structures exist, either cubic $Pm\bar{3}m$ (Mao et al. 1989; Tamai and Yagi 1989; Wang et al. 1996; Shim et al. 2000) or tetragonal (Shim et al. 2002; Ono et al. 2004). $CaSiO_3$ perovskite has also instigated several theoretical calculations (Stixrude et al. 1996; Chizmeshya et al. 1996; Warren et al. 1998; Magyari-Kope et al. 2002a, b; Akber-Knutson et al. 2002; Jung and Oganov 2005; Caracas et al. 2005), and is found to be *Pnam* and *I*4/*mcm* at pressures above 14.2 GPa at 0 K. For a review of these calculations, see Jung and Oganov (2005). A variety of physical properties such as high temperature, high pressure properties, in particular elasticity (Adams and Oganov 2006; Li et al. 2006), trace element incorporation (Corgne et al. 2003), melting behaviour (Wang 1999) and solubility with

$MgSiO_3$ (Kesson et al. 1995; Watson et al. 2000; Vitos et al. 2006) have been investigated using theoretical calculations.

The previous studies on reciprocal solubilities in the two perovskites have shown the following: According to Kesson et al. (1995), the solid solution of $MgSiO_3$–$CaSiO_3$ perovskite is extremely limited because of the size difference of the cations. Ca^{2+} is in fact >25% larger than both the silicon and the magnesium, thus Kesson et al. (1995) found it unlikely that Ca will enter the $MgSiO_3$ perovskite structure to any significant degree. This difference in ionic size was calculated according to a scheme based on bond strengths, coordination number and single crystal measurements.

Watson et al. (2000) employed an atomistic simulation method based on the Born model of solids in which the individual interactions are defined by interatomic potentials. They calculated the Ca partitioning within the lower mantle through the solution energy of Ca in $MgSiO_3$. In the pressure and temperature range of the lower mantle, a $Ca_{0.5}Mg_{0.5}SiO_3$ perovskite is shown to be extremely unfavourable and Watson et al. (2000) argue that almost all of the Ca would prefer to form its own $CaSiO_3$ perovskite phase.

Vitos et al. (2006) combined density functional theory within the generalized gradient approximation (GGA) with simulations employing the exact muffin-tin orbitals and with the projector-augmented wave (PAW) method. They calculated the energy of formation for $(Mg,Ca)SiO_3$ perovskite and $(Mg,Ca)_3(MgSi)Si_3O_{12}$ garnet solid solutions. Vitos et al. (2006) found that a $Mg_{1-x}Ca_xSiO_3$ perovskite solid solution with $x \approx 0.04$–0.06 would be stable at the transition zone base and in the uppermost lower mantle, and that with increasing pressure the extent of solid solution would decrease and both perovskites approach endmember compositions.

Studies on the $MgSiO_3$–Al_2O_3 system (Panero et al. 2006; Tsuchiya and Tsuchiya 2008; Jung et al. 2010) show quite a different behaviour and result in extensive solid solution between $MgSiO_3$ and Al_2O_3. All these studies employ density functional theory but differ in their approach treating statistical effects. Due to the high sophistication required to deal with the statistical effects, they are computationally expensive.

In this work, phase compositions in the lower mantle, i.e. the solid solution(s) of the $MgSiO_3$ and the $CaSiO_3$ perovskites, are calculated. This study follows a previous one where the stability and decomposition of pure $CaSiO_3$ perovskite (Jung and Oganov 2005) were investigated. Quantum mechanical simulations are a feasible way to perform structural studies at lower mantle pressures. Based on these structural data and on resulting solution energies, thermodynamic modelling is performed to better understand the lower mantle phase relations which only involve low reciprocal concentrations of Ca or Mg in the perovskites. In this study, a substitutional solid solution of Mg and Ca in the silicate perovskite framework was considered, although other elements which occur naturally in the lower mantle, such as Al and Fe, were not included at this stage.

Methodology

The present calculations have been performed with the VASP (Vienna ab initio simulation package) (Kresse and Furthmuller 1996) code. The GGA (Perdew et al. 1996) together with the PAW (Blöchl 1994; Blöchl et al. 2003) method have been used to calculate energies of the different structures at 0 K. In all calculations, the following PAW potentials were used: Core region cut-offs are 2.3 atomic units (a.u.) for calcium (core configuration $1s^2 2s^2 p^6$, $3s^2 3p^6 4s^2$ as valence), 1.5 a.u. for silicon (core configuration $1s^2 2s^2 p^6$, $3s^2 p^2$ as valence), 1.52 a.u. for oxygen (core configuration $1s^2$, $2s^2 p^4$ as valence) and 2.0 a.u. for magnesium (core configuration $1s^2 2s^2$, $2p^6 3s^2$ as valence).

A plane wave cut-off energy of 500 eV for all calculations proved to be reliable (convergence of energy to within 2×10^{-3} eV per formula unit, convergence of pressure to within 0.4 GPa) and computationally acceptable. The energy differences converge to within 8×10^{-4} eV. For the Brillouin zone sampling, the Monkhorst–Pack scheme (Monkhorst and Pack 1976) was used, and convergence of energy and stress with respect to the mesh density was tested for each structure individually.

All perovskite structures do consist of a 160 atom cell (32 formula units, f.u.), and the *k*-point sampling was done with a $2 \times 2 \times 2$ Monkhorst–Pack grid. The ions were relaxed with the conjugate gradient and the steepest descent methods. The energy minimization procedure is iterative and proceeds until self-consistency within a prescribed tolerance of 10^{-4} eV per unit cell for electronic optimization and 10^{-3} eV per unit cell for ionic relaxation.

For the description of the solid solution, a subregular substitutional solid solution model with Margules parameters (Table 1) was used, which is based on point defect calculations. A complete description of the enthalpy of every mixture of the two endmembers is needed to model the solubility. Calculating the energies and structures of many different compositions with ab initio methods is computationally rather expensive, additionally there are different possibilities to arrange the solid solution atom assembly within a single composition. Therefore, an approach, which allows the modelling of the enthalpy in the entire relevant compositional range with only four ab initio calculations, was used. These were the endmembers

Table 1 Margules parameters of enthalpy for *Pnma* in kJ/mol% (Q_1 and Q_2) and for *I4/mcm* (Q_{1B}), volume Margules parameters for *Pnam* (Q_{vmix1} and Q_{vmix2}) in V^3/mol% and for *I4/mcm* (Q_{vmix1B})

Pressure (GPa)	Q_1	Q_2	Q_{1B}	Q_{vmix1}	Q_{vmix2}	Q_{vmix1B}
25	110.55	98.15	29.67	58.31	40.45	23.87
30	119.46	106.68	39.31	46.73	36.84	21.10
40	120.40	114.72	44.05	38.65	38.65	29.67
50	137.06	121.59	48.33	52.01	36.18	19.19
60	145.18	128.93	52.14	47.25	43.92	20.34
70	153.60	135.94	53.91	39.80	38.48	8.39
80	160.79	142.98	55.65	40.54	37.74	8.35
90	167.36	149.87	58.67	33.62	35.42	16.79
100	174.51	156.37	61.39	39.54	39.08	10.81
110	180.90	163.30	63.91	40.31	28.40	6.02
120	187.68	169.62	65.41	35.81	28.94	11.59
130	194.81	176.36	66.46	33.01	28.10	8.42
140	200.92	182.64	68.74	28.61	29.20	8.79

(pure $CaSiO_3$ and $MgSiO_3$ perovskite) and two point defect structures ($Ca_{31}MgSi_{32}O_{96}$ and $Mg_{31}CaSi_{32}O_{96}$ perovskite). The excess enthalpy relative to a mechanical mixture of the two endmembers is the enthalpy of mixing $H_{\text{excess-mix}}$. The four points are denoted with crosses in Fig. 1a. The $H_{\text{excess-mix}}$ of a point defect is defined as:

$$H_{\text{excess}-\text{mix}}(x') = H_{\text{pointdefect}-x'} - x' \times (H_2 - H_1), \quad (1)$$

where x' is the molar fraction of endmember 2, $H_{\text{pointdefect}-x'}$ the enthalpy of the point defect at the composition x', H_1 and H_2 are the enthalpies of the pure endmembers. The second term on the right is the mechanical mixing energy between endmembers 1 and 2, denoted as dashed line in Fig. 1a.

For the mathematical form of the enthalpy of mixing, a subregular solid solution model was used, where the excess mixing enthalpy $H_{\text{excess-mix}}$ of the mixture for the entire compositional range is given by

$$H_{\text{excess}-\text{mix}}(x) = x \times (1-x)(Q_2 \times x + Q_1(1-x)). \quad (2)$$

The Margules parameters Q_1 and Q_2 of $H_{\text{excess-mix}}(x)$ together with the data points of the two $H_{\text{excess-mix}}(x')$ are used to define a set of linear equations. This can be solved for Q_1 and Q_2. The excess mixing enthalpy is then added to the mechanical mixture and the enthalpy $H(x)$ is given by

$$H(x) = (H_2 - H_1) \times x + H_1 + H_{\text{excess}-\text{mix}}. \quad (3)$$

These calculations have been performed at 0 K, and so to study finite-temperature solubilities temperature effects were introduced through the entropy. Entropy in our model consists of two parts, the configurational entropy of random mixing:

$$S_{\text{conf}}(x) = R(x \times \ln(x) + (1-x) \times \ln(1-x)), \quad (4)$$

where R is the gas constant, and the vibrational entropy (Urusov 1987; Oganov and Price 2005):

$$S_{\text{vib}-\text{excess}}(x) = \gamma \times C_V \times \Delta V/V_0 + \sum_i n_i R \ln \sqrt{\frac{v_i}{v_{0i}}}, \quad (5)$$

where γ is the Grüneisen parameter, C_V is the heat capacity, $\Delta V/V_0$ is the relative change in volume and v_i and v_{0i} are the coordination numbers. The term including the coordination numbers is zero, because this is the vibrational excess entropy within one structure type, thus the coordination number stays the same and the relative difference cancels through the mechanical mixing. At high temperatures (above the Debye temperature), the heat capacity C_V can be approximated in the Dulong–Petit limit with:

$$C_V = 3nR \quad (6)$$

The Grüneisen parameter γ was fixed at 1.5 for all temperatures (Adams and Oganov 2006; Oganov et al. 2001a, b). At a given pressure, the Gibbs free energy is then given by

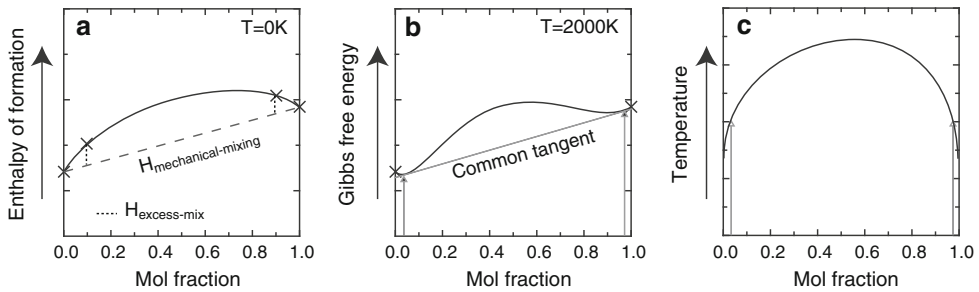

Fig. 1 Schematics of the method employed to calculate the complete perovskite solid solution. **a** Model the enthalpy through four ab initio calculations, **b** introduce temperature effects through entropy, find common tangent and coexisting phase compositions, **c** plot compositions at different temperatures to constitute the complete solvus. It should be noted that this method is precise in the vicinity of the calculated compositions, which cover the compositional range of interest

$$G(x) = H(x) - T(S_{\text{vib}} + S_{\text{conf}}). \quad (7)$$

The limit of solid solution is found where two phases coexist, i.e. where they are in thermodynamic equilibrium and the chemical potentials $\mu(P, T, n)$ of all the components in both phases are the same. The chemical potential is given by the derivative of the Gibbs free energy with respect to the composition $\partial G/\partial x$, hence, Eq. 8 must be fulfilled

$$\frac{\partial G(x)}{\partial x_1} = \frac{\partial G(x)}{\partial x_2}. \quad (8)$$

For a given temperature, two compositions with identical chemical potential have identical slopes of the Gibbs free energy curves in G–x space. Using the common tangent method (Fig. 1b), every temperature yields two compositions, which in turn define the solvus curve (Fig. 1c). To solve this equation system, an algorithm written in Mathematica (Wolfram Research Inc 2007) was used and a numerical minimization of the Gibbs free energy was performed.

To model the excess mixing enthalpy as described above (Fig. 1) is only possible if the complete solid solution has the same symmetry and thus there is one continuous G–x curve. Since this is generally not the case for $CaSiO_3$ (*I4/mcm*) and $MgSiO_3$ (*Pnma*) perovskites, two solid solution G-surfaces have to be calculated, each including an existing endmember and a virtual one. For our system, one G-surface describes the excess mixing enthalpy of $CaSiO_3$ in $MgSiO_3$ with the space group 62 ($CaSiO_3$ in *Pnam* and $MgSiO_3$ in *Pnma*) and a second G-surface for the space group 140 (*I4/mcm*). The structures of the space group 62 and 140 are competing, and the phase transition takes place at the crossover of the curves (Fig. 2)

$$G_{Pnma}(x_0) = G_{I4/mcm}(x_0). \quad (9)$$

The Gibbs free energy minimum surface is then defined such that it consists of one symmetry up to the point x_0, where the phase transition takes place, and of the other symmetry at $x > x_0$, resulting in a definition of the Gibbs free energy of the system in two segments.

$$G_{\text{total}} = \begin{cases} G_{I4/mcm}, & \text{if } 0 < x < x_0 \\ G_{Pnma}, & \text{if } x_0 < x < 1 \end{cases}. \quad (10)$$

The common tangent onto this Gibbs energy curve will yield the two coexisting phases with two different symmetries and with Margules parameters based on the defect energy modelling. This approach to model the mixing properties has been already used for many other phases (Wohl 1946, 1953; Redlich and Kister 1948; Cheng and Ganguly 1994) and enables with relatively few ab initio calculations a good treatment of the solvi of mineral mixtures.

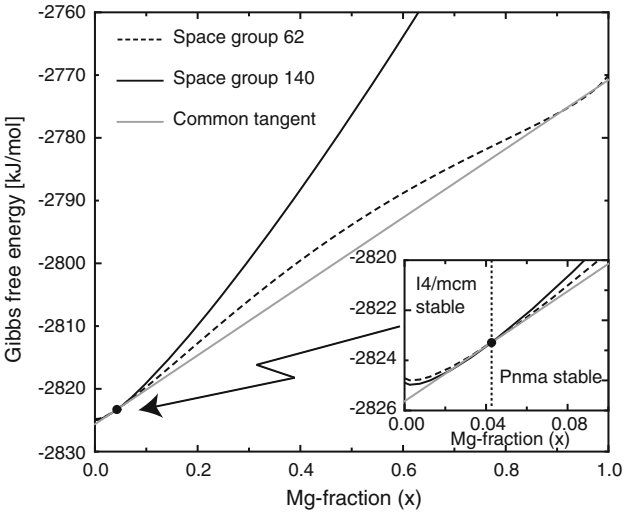

Fig. 2 Gibbs free energy of the perovskite solid solution at 3,000 K, 25 GPa. *Solid line* Space group 140 structure type, *dashed line* space group 62 structure type. The composition of (metastable) coexistence of the two structures is defined by the crossover, *left* of the black dot *I4/mcm* is (meta-)stable, *right* of it *Pnma*. The *gray line* is the common tangent onto the stable structures

Finally, a word of caution is necessary: Our approach does not include energetic contributions from order–disorder phenomena. Potentially, such effects could be significant for reciprocal concentrations of Ca and Mg in the perovskites that are much larger than those calculated for any reasonable geotherm in the Earth. Secondly, absolute temperatures for reciprocal solubilities of >5 mol% are 3,000–6,000 K and it is questionable if ordering would occur at such temperatures. Consequently, as ordering in the perovskites does not appear to be relevant for the Earth mantle, we have not undertaken such calculations.

The $CaSiO_3$–$MgSiO_3$ perovskite solid solution

The structures and energies of the pure $CaSiO_3$ and $MgSiO_3$ perovskites were calculated, together with their respective substitutional point defects. Figure 3 depicts the relaxed and optimized structures of the two point defect structures. Although minor local distortions can be observed, the overall structure is conserved, i.e. the tilting of the Si–O octahedra remains the same. This also holds with increasing pressure.

For the orthorhombic structures, the asymmetric description of the Gibbs free energy was used, i.e. 4 points were used to fit the excess energy. For the tetragonal structures only the pure endmembers and the $CaSiO_3$ perovskite Mg point defect structure were used to fit the excess energy. The $MgSiO_3$ perovskite Ca point defect was not usable as excessive distortions of the cell lead to a

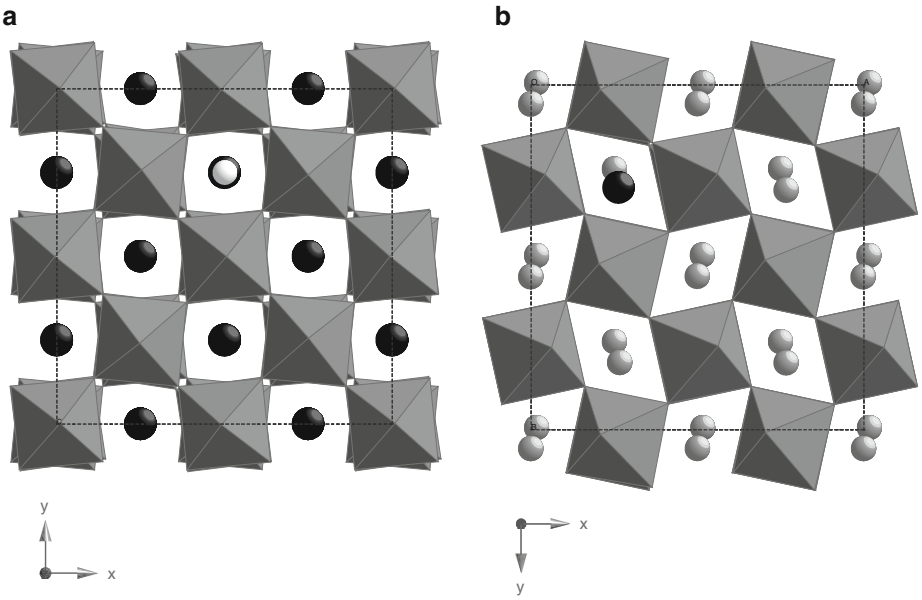

Fig. 3 Supercell with 160 atoms (32 f.u.) containing 1 substitutional defect: **a** $CaSiO_3$ perovskite in the *I4/mcm* symmetry; **b** $MgSiO_3$ perovskite in the *Pnma* symmetry; Ca atoms are represented as *black spheres*, Mg as *grey spheres*, and the *grey octahedra* are the Si–O octahedra, structures correspond to 30 GPa

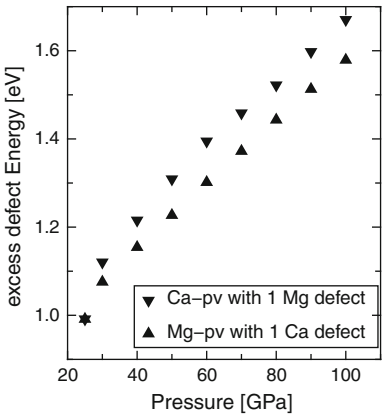

Fig. 4 Defect energies of the perovskite structures, relative to the mechanical mixture of the pure perovskites at 0 K temperature. At 25 GPa, both defect energies plot on top of each other

different structure type, invalidating the initial scope of modelling the tetragonal structure across the entire compositional range. Nevertheless, the details of the Mg-rich side of the tetragonal perovskite mixing enthalpy do not have any perceivable influence on the minimum G_{total} surface of the perovskites (see Fig. 2).

Figure 4 shows the point defect energies of the structures at Earth mantle pressures. The defect energies are the excess energies compared to the mechanical mixture of the pure endmembers (Eq. 1). For both structures, at low pressure (25 GPa), it is equally unfavourable to incorporate a substitutional point defect, the excess defect energy being almost identical. As pressure increases, the point defect energies diverge and the energy cost to incorporate a Mg atom into the Ca-perovskite framework becomes higher than the energy cost for a Ca atom to be incorporated into $MgSiO_3$ perovskite. The size difference of the ionic radii alone would actually imply the reverse, since Ca^{2+} is much bigger than Mg^{2+}. However, the structure of the $MgSiO_3$ perovskite is more flexible to incorporate defects than the $CaSiO_3$ perovskite structure, which is of higher symmetry and thus reacts more to distortions and symmetry violations.

Figure 5 shows the solvi of the $CaSiO_3$–$MgSiO_3$ perovskite solid solution at pressures from 25 to 100 GPa. The left hand side of the graph, which consists of $CaSiO_3$ with a certain amount of Mg incorporated, shows a visible kink at 3,100 K and 25 GPa. This jump in solubility is caused by the phase transition from the *I4/mcm* to the *Pnam* phase. As illustrated in Fig. 2, there are two competing structures: In the case of $CaSiO_3$, these structures are energetically close to each other, and the enthalpy difference is only a few meV/f.u. (Jung and Oganov 2005). The phase transition in $CaSiO_3$ perovskite causes a discontinuous increase in solubility at the transition temperature, due to the coexistence of the two $CaSiO_3$ phases. Below this temperature, there is a solid solution of *I4/mcm* $CaSiO_3$ perovskite coexisting with a solid solution of *Pnma* $MgSiO_3$ perovskite, above this temperature both perovskites have *Pnma* symmetry. The discontinuity in the solubility shifts with increasing pressure from 5% at 25 GPa, 3,100 K to lower Mg concentrations of 2.5% at 100 GPa, 4,400 K (Fig. 5).

The Mg-rich half of the two perovskite $(Ca,Mg)SiO_3$ system is compositionally equivalent to the $Mg_2Si_2O_6$–$CaMgSi_2O_6$ enstatite–diopside join at lower pressures. Both systems have in common, that the solvus opens with pressure, indicating that mixing of Ca and Mg on a single site (the M2 site in pyroxenes) is volumetrically less favourable than coexistence of the pure endmembers (Brey and Huth

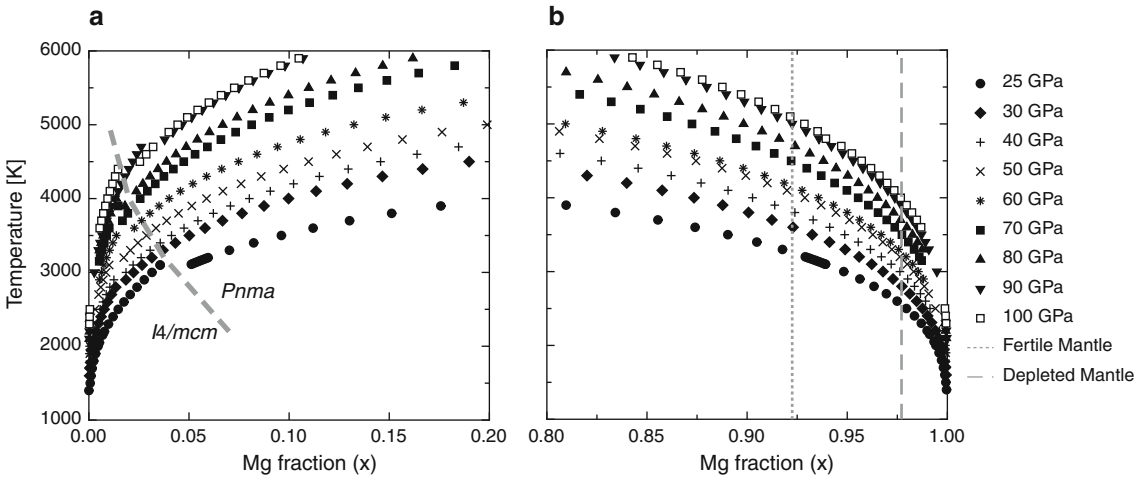

Fig. 5 Solvus of $CaSiO_3$–$MgSiO_3$ perovskites at Earth mantle pressures. For a better resolution, the solvus is split in **a** Ca-rich and **b** Mg-rich part

1984; Gasparik 2003). On the other hand, the reciprocal solubilities of Mg and Ca on the M2 site of the pyroxenes are much higher than the reciprocal solubilities in the perovskites. Furthermore, in the pyroxenes, the asymmetry of the reciprocal solubilities is in favour of incorporation of the smaller Mg into the Ca (M2) site of diopside, leading to pigeonites with as much as 75 mol% replacement of Ca by Mg in the M2 site, while the solubility of Ca in clino- or ortho-enstatite typically amounts to 5 mol% in the M2 site, contrasting the perovskite solid solution.

The solubility of Ca in $MgSiO_3$ at 25 GPa is as low as 0.5% at 2,000 K, but increases with temperature to 5% at 3,000 K. In general, the Ca solubility in $MgSiO_3$ perovskite is higher than that of Mg in $CaSiO_3$ perovskite. With increasing pressure, the solubility of both phases decreases, and the solvus opens up with pressure (Fig. 6). Up to now, there are no experiments on coexisting perovskites in the $CaSiO_3$–$MgSiO_3$ (or any other simple) system. Thus, our predictions on the compositions and solvus of the perovskites in the lower mantle cannot be compared to experimental values. Figure 7 shows isopleth of Ca in $MgSiO_3$ perovskites coexisting with Ca-perovskite, i.e. solubility in terms of $(Mg_{1-x}Ca_x)SiO_3$ perovskite compositions at lower mantle pressures and temperatures. The compositions are compared to lower mantle adiabats of da Silva et al. (2000) and Turcotte and Schubert (2002). At temperatures and pressures of the lower mantle, even for a relatively elevated adiabat such as that of da Silva et al. (2000), a maximum of 1–2% of Ca can be incorporated into the $MgSiO_3$ perovskite. This is far below the Ca/(Ca + Mg) or Ca/(Ca + Mg + Fe) fraction of any average mantle composition, and therefore $CaSiO_3$ perovskite should coexist with $MgSiO_3$ as a separate phase over the entire depth range of the Earth mantle.

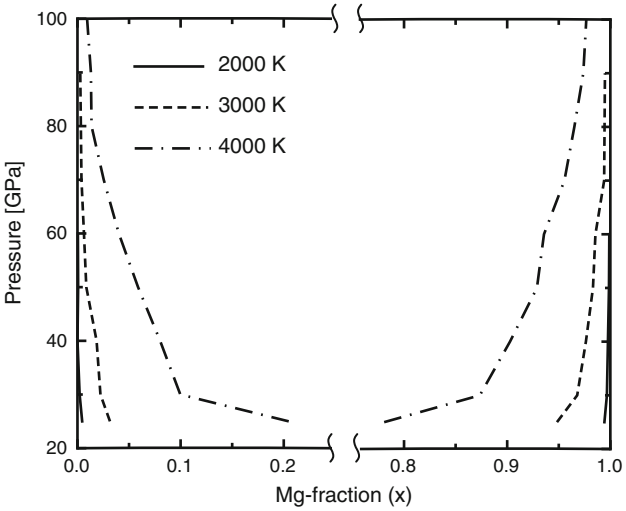

Fig. 6 Solubility of $CaSiO_3$–$MgSiO_3$ perovskite solid solution at pressures and temperatures relevant for the Earth mantle

Beside the adiabat, a second temperature profile through the mantle is of major interest to geochemistry, i.e. the solidus of the lower mantle. The question to be addressed is whether there would be $CaSiO_3$ perovskite present at the solidus, and thus possibly be a residuum to small degrees of melting in the lower mantle. This question is of particular relevance to melt geochemistry, as many trace elements may be retained in Ca-perovskite but not in Mg-perovskite, solid/melt partition coefficients for many geochemically important traces (REE, U, Th) being ≥2 orders of magnitude higher for Ca-perovskite than for Mg-perovskite (Corgne et al. 2003). Figure 7b gives Ca solubilities in terms of molar fraction along a geotherm and along the lower mantle solidus of Zerr et al. (1998). Along the solidus, approximately 0.03 Ca can be incorporated into $MgSiO_3$ perovskite

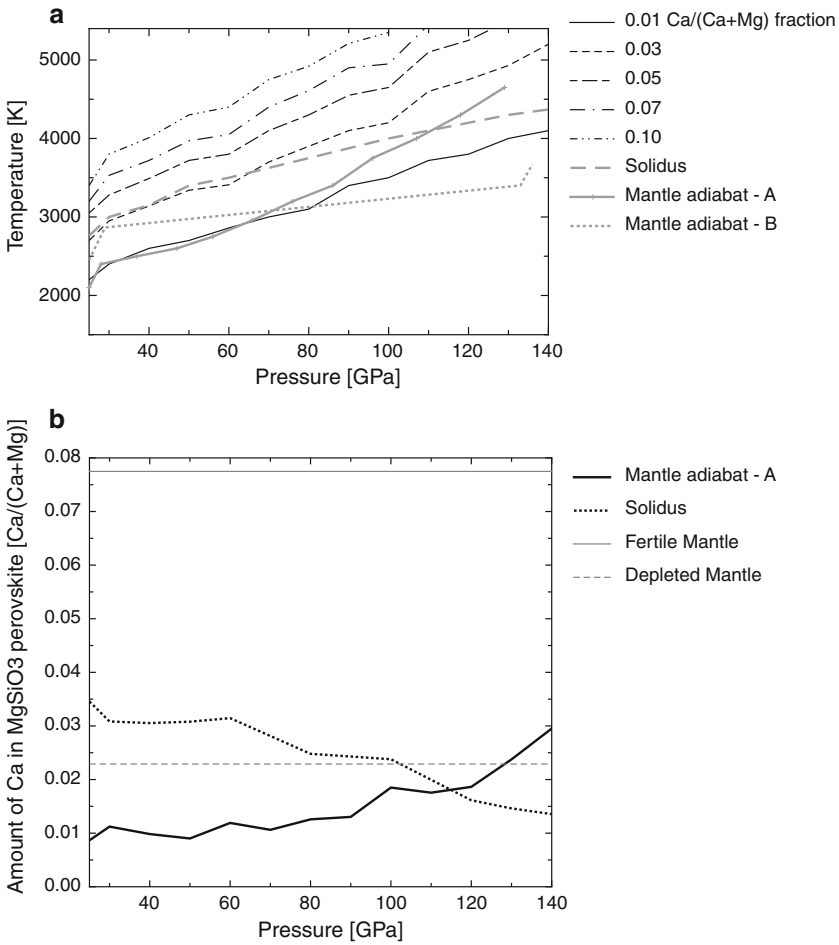

Fig. 7 **a** Isopleth of molar Ca fraction in $MgSiO_3$ perovskite compared to different mantle adiabats A (da Silva et al. 2000), B (Turcotte and Schubert 2002) and solidus (Zerr et al. 1998). Following any geotherm, <1 mol% Ca will be incorporated into $MgSiO_3$ perovskite in the uppermost lower mantle, and at most 2 mol% when approaching the D" layer. **b** Calculated Ca fractions at solidus and geotherm temperatures compared to Ca fractions of fertile and depleted mantle (*horizontal lines*)

at pressures of 25–60 GPa. For a fertile pyrolytic mantle composition, this would be insufficient to dissolve all $CaSiO_3$ perovskite into $MgSiO_3$ perovskite. Hence at the expected low degrees of melting, Ca-perovskite will remain residual in fertile (pyrolytic) mantle. Nevertheless, a depleted harzburgitic mantle with less than 1.25 wt% CaO will loose the Ca-perovskite before reaching the solidus.

Vitos et al. (2006) obtained that at pressures of the uppermost lower mantle, a solid solution of $(Mg_{1-x}Ca_x)SiO_3$ with $x \approx 0.04$–0.06 is stable. The difference in method to Vitos et al. (2006) is that they employed fixed discrete compositions and investigated their stability with respect to a decomposition into the pure perovskite end-members, whereas we investigated the relevant compositional range of all the pressures and temperatures within our assumptions.

Conclusions

This study demonstrates that along any reasonable mantle adiabat, the two-perovskite solvus in the $(Ca,Mg)SiO_3$ system will widen rather than narrow, and thus, two perovskites are to be expected in fertile mantle compositions throughout the entire lower mantle. Whether this holds for more complex systems in which Al, Fe^{3+}, and Fe^{2+} as well as Na will be incorporated into the perovskite structures remains to be demonstrated. In analogy to the pyroxenes, and at the expected concentrations of Al, Fe, and Na in the perovskites, we do not expect a significant closure of the solvus at adiabatic temperatures, but a considerable decrease in the temperature of the solvus' crest, which is of little practical significance as these temperatures are far beyond any expected mantle temperature. Regarding Al, calculations on the $CaSiO_3$–$MgSiO_3$ perovskite solvus with aluminium impurities are presently in progress.

Acknowledgments We thank ETH Zurich for funding, the CSCS Manno for access to supercomputers, A.R. Oganov for advising during this study and for a critical review of an earlier version of the manuscript, and W. Steurer for his generous support of this study. We also thank M. Walter and an anonymous reviewer for helpful comments and constructive criticism.

References

Adams DJ, Oganov AR (2006) Ab initio molecular dynamics study of $CaSiO_3$ perovskite at *P–T* conditions of Earth's lower mantle. Phys Rev B 73(18):184–106

Akber-Knutson S, Bukowinski MST, Matas J (2002) On the structure and compressibility of $CaSiO_3$ perovskite. Geophys Res Lett 29(3):1034

Anderson DL (1989) Theory of the Earth. Blackwell Publications, Boston

Blöchl PE (1994) Projector augmented-wave method. Phys Rev B 50(24):17953–17979

Blöchl PE, Forst CJ, Schimpl J (2003) Projector augmented wave method: ab initio molecular dynamics with full wave functions. Bull Mater Sci 26(1):33–41

Brey G, Huth J (1984) The enstatite–diopside solvus to 60 kbar. In: Proceedings of the third international Kimberlite conference, vol 2, pp 257–264

Caracas R, Wentzcovitch R, Price GD, Brodholt J (2005) $CaSiO_3$ perovskite at lower mantle pressures. Geophys Res Lett 32(6):L06306

Cheng WJ, Ganguly J (1994) Some aspects of multicomponent excess free-energy models with subregular binaries. Geochim Cosmochim Acta 58(18):3763–3767

Chizmeshya AVG, Wolf GH, McMillan PF (1996) First-principles calculation of the equation-of-state, stability, and polar optic modes of $CaSiO_3$ perovskite. Geophys Res Lett 23(20):2725–2728

Corgne A, Allan NL, Wood BJ (2003) Atomistic simulations of trace element incorporation into the large site of $MgSiO_3$ and $CaSiO_3$ perovskites. Phys Earth Planet Interiors 139(1–2):113–127

da Silva CRS, Wentzcovitch RM, Patel A, Price GD, Karato SI (2000) The composition and geotherm of the lower mantle: constraints from the elasticity of silicate perovskite. Phys Earth Planet Interiors 118(1–2):103–109

Gasparik T (2003) Phase diagrams for geoscientist. Springer, Berlin

Green DH, Hibberson WO, Jaques AL (1979) Petrogenesis of mid-ocean ridge basalts. In: McElhinny M (ed) The Earth: its origin, structure, and evolution. Academic Press, New York

Hirose K, Shimizu N, van Westrenen W, Fei Y (2004) Trace element partitioning in earth's lower mantle and implications for geochemical consequences of partial melting at the core–mantle boundary. Phys Earth Planet Interiors 146(1–2):249–260

Jung DY, Oganov AR (2005) Ab initio study of the high-pressure behavior of $CaSiO_3$ perovskite. Phys Chem Miner 32(2):146–153

Jung DY, Vinograd VL, Fabrichnaya OB, Oganov AR, Schmidt MW, Winkler B (2010) Thermodynamics of mixing in $MgSiO_3$–Al_2O_3 perovskite and ilmenite from ab initio calculation. Earth Planet Sci Lett 295(3–4):477–486

Kesson SE, Fitz Gerald JD, Shelley JMG, Withers RL (1995) Phase-relations, structure and crystal-chemistry of some aluminous silicate perovskites. Earth Planet Sci Lett 134(1–2):187–201

Kresse G, Furthmuller J (1996) Efficient iterative schemes for ab initio total-energy calculations using a plane-wave basis set. Phys Rev B 54(16):11169–11186

Li L, Weidner DJ, Brodholt J, Alfe D, Price GD, Caracas R, Wentzcovitch R (2006) Elasticity of $CaSiO_3$ perovskite at high pressure and high temperature. Phys Earth Planet Interiors 155(3–4):249–259

Magyari-Kope B, Vitos L, Grimvall G, Johansson B, Kollar J (2002a) Low-temperature crystal structure of $CaSiO_3$ perovskite: an ab initio total energy study. Phys Rev B 65(19):193107/1–4

Magyari-Kope B, Vitos L, Johansson B, Kollar J (2002b) Model structure of perovskites: cubic–orthorhombic phase transition. Comput Mater Sci 25(4):615–621

Mao HK, Chen LC, Hemley RJ, Jephcoat AP, Wu Y, Bassett WA (1989) Stability and equation of state of $CaSiO_3$-perovskite to 134-GPa. J Geophys Res Solid Earth 94(B12):17889–17894

Monkhorst HJ, Pack JD (1976) Special points for Brillouin-zone integrations. Phys Rev B 13:5188–5192

Oganov AR, Price GD (2005) Ab initio thermodynamics of $MgSiO_3$ perovskite at high pressures and temperatures. J Chem Phys 122:art.124501

Oganov AR, Brodholt JP, Price GD (2001a) Ab initio elasticity and thermal equation of state of $MgSiO_3$ perovskite. Earth Planet Sci Lett 184(3–4):555–560

Oganov AR, Brodholt JP, Price GD (2001b) The elastic constants of $MgSiO_3$ perovskite at pressures and temperatures of the Earth's mantle. Nature 411(6840):934–937

O'Neill B, Jeanloz R (1990) Experimental petrology of the lower mantle—a natural peridotite taken to 54 GPa. Geophys Res Lett 17(10):1477–1480

Ono S, Ito E, Katsura T (2001) Mineralogy of subducted basaltic crust (morb) from 25 to 37 GPa, and chemical heterogeneity of the lower mantle. Earth Planet Sci Lett 190(1–2):57–63

Ono S, Ohishi Y, Mibe K (2004) Phase transition of Ca-perovskite and stability of Al-bearing Mg-perovskite in the lower mantle. Am Mineral 89(10):1480–1485

Panero WR, Akber-Knutson S, Stixrude L (2006) Al_2O_3 incorporation in $MgSiO_3$ perovskite and ilmenite. Earth Planet Sci Lett 252(1–2):152–161

Perdew JP, Burke K, Ernzerhof M (1996) Generalized gradient approximation made simple. Phys Rev Lett 77(18):3865–3868

Redlich O, Kister AT (1948) Thermodynamics of nonelectrolyte solutions—*x*–*y*–*t* relations in a binary system. Ind Eng Chem 40(2):341–345

Shim SH, Duffy TS, Shen GY (2000) The stability and *P*–*V*–*T* equation of state of $CaSiO_3$ perovskite in the Earth's lower mantle. J Geophys Res Solid Earth 105(B11):25955–25968

Shim SH, Jeanloz R, Duffy TS (2002) Tetragonal structure of $CaSiO_3$ perovskite above 20 GPa. Geophys Res Lett 29(24):2166

Stixrude L, Cohen RE, Yu RC, Krakauer H (1996) Prediction of phase transition in $CaSiO_3$ perovskite and implications for lower mantle structure. Am Mineral 81(9–10):1293–1296

Tamai H, Yagi T (1989) High-pressure and high-temperature phase-relations in $CaSiO_3$ and $CaMgSi_2O_6$ and elasticity of perovskite-type $CaSiO_3$. Phys Earth Planet Interiors 54(3–4):370–377

Taura H, Yurimoto H, Kato T, Sueno S (2001) Trace element partitioning between silicate perovskites and ultracalcic melt. Phys Earth Planet Interiors 124(1–2):25–32

Tsuchiya J, Tsuchiya T (2008) Postperovskite phase equilibria in the $MgSiO_3$–Al_2O_3 system. Proc Natl Acad Sci USA 105(49):19160–19164

Turcotte DL, Schubert G (2002) Geodynamics. Cambridge University Press, Cambridge

Urusov VS (1987) Theoretical Crystal Chemistry. Moscow State University Press, Moscow, p 275

Vitos L, Magyari-Kope B, Ahuja R, Kollar J, Grimvall G, Johansson B (2006) Phase transformations between garnet and perovskite phases in the Earth's mantle: a theoretical study. Phys Earth Planet Interiors 156(1–2):108–116

Wang YB, Weidner DJ, Guyot F (1996) Thermal equation of state of $CaSiO_3$ perovskite. J Geophys Res Solid Earth 101(B1):661–672

Wang ZW (1999) The melting of Al-bearing perovskite at the core–mantle boundary. Phys Earth Planet Interiors 115(3–4):219–228

Warren MC, Ackland GJ, Karki BB, Clark SJ (1998) Phase transitions in silicate perovskites from first principles. Mineral Mag 62(5):585–598

Watson GW, Wall A, Parker SC (2000) Atomistic simulation of the effect of temperature and pressure on point defect formation in $MgSiO_3$ perovskite and the stability of $CaSiO_3$ perovskite. J Phys Condens Matter 12(39):8427–8438

Wohl K (1946) Thermodynamics evaluation of binary and ternary liquid systems. Trans Am Inst Chem Eng 42(2):215–249
Wohl K (1953) Thermodynamic evaluation of binary and ternary liquid systems. Chem Eng Progr 49(4):218–219
Wolfram Research Inc (2007) Mathematica Version 6. Wolfram Research Inc, Champaign, IL
Zerr A, Diegeler A, Boehler R (1998) Solidus of Earth's deep mantle. Science 281(5374):243–246